J. Cent. South Univ. (2018) 25: 1285−1294
DOI: https://doi.org/10.1007/s11771-018-3825-5

Springer

Effect of ultrasonic field on microstructure and mechanical properties of as-cast 7085 aluminum alloy

ZOU Hao(邹浩)[1], PAN Qing-lin(潘清林)[1, 2], SHI Yun-jia(史运嘉)[1], CHEN Jing(陈婧)[1], XIANG Hao(向浩)[1], LI Rui-shi(李瑞师)[2], LI Hang(李航)[2]

1. School of Materials Science and Engineering, Central South University, Changsha 410083, China;
2. Suntown Technology Group Co., Ltd, Changsha 410200, China

Abstract: The effect of an ultrasonic field on the microstructure and mechanical properties of 7085 aluminum alloy during solidification was investigated by optical microscopy, Vickers hardness test, tensile test, scanning electron microscopy (SEM) with energy dispersive X-ray spectrometry, and electron probe micro-analysis (EPMA). The results showed that the grains of aluminum alloy were significantly refined and secondary phases were dispersed and distributed uniformly at the grain boundaries, due to ultrasonic treatment (UST). By EPMA, it was observed that the distribution of the main elements Al, Zn, Mg and Cu was more homogeneous in alloys with UST, than in alloys without UST. The mechanical properties of the aluminum alloy also significantly improved. As demonstrated by the SEM fractography of the fractured faces of several castings, fracture of the unrefined specimens occurred in a brittle manner, whereas the cracks of the refined specimens showed quasi-cleavage fracture.

Key words: ultrasonic treatment; grain refinement; microstructure; secondary phases

Cite this article as: ZOU Hao, PAN Qing-lin, SHI Yun-jia, CHEN Jing, XIANG Hao, LI Rui-shi, LI Hang. Effect of ultrasonic field on microstructure and mechanical properties of as-cast 7085 aluminum alloy [J]. Journal of Central South University, 2018, 25(6): 1285–1294. DOI: https://doi.org/10.1007/s11771-018-3825-5.

1 Introduction

Al–Zn–Mg–Cu alloys are widely used in the aerospace industry due to their high strength, high toughness, and good ductility in operation [1–3]. However, conventionally cast ingots have some defects, such as microstructure coarseness and dendritic segregation, which can lead to subsequent plastic deformation and poor machining [4]. In order to obtain good workability and service performance of alloys, various methods including refiner addition, electronic-magnetic stirring [5], and ultrasonic vibration [6], have been used in the process of casting. As a simple and potential physical method, ultrasonic treatment (UST) has proven to be effective in refining metal grains [7]. Compared to other approaches, UST has some advantages: it does not introduce any impurities because it is a purely physical process [8], it is simple and can be used for industrial production, and it is environmentally friendly. Thus, the ultrasonic vibration method has great potential for industrial application.

Recently, researchers have been paying closer attention to the use of ultrasound in metal-forming processes. However, researchers have varied views on the effect of ultrasound on grain refinement. This is because the melt inside the crucible is opaque, and hence, changes in the microstructure cannot be observed directly. ESKIN et al [9] reported that cavitation in melt aluminum caused by ultrasonic

Foundation item: Project(2016GK1004) supported by the Science and Technology Major Project of Hunan Province, China
Received date: 2016−12−19; **Accepted date:** 2017−03−06
Corresponding author: PAN Qing-lin, PhD, Professor; Tel: +86–731–88830933; E-mail: pqlcsu1@163.com

sound can increase the wettability and promote nucleation. YASUDA et al [10] considered that ultrasonic vibrations can break up the primary dendrites. JIANG et al [11] investigated the response of 7085 aluminum alloy to ultrasonic vibration and concluded that the grain refinement was due to the combined effect of cavitation-promoted nucleation and the dissolution of Ti from the eroding radiator. Apart from grain refinement, UST can also be applied to degas the melt. Introduction of ultrasonic sound can effectively eliminate porosity, which is one of the major defects in aluminum alloy castings [12].

This study reports the results of carefully designed experiments in which ultrasonic sound was introduced in the melt aluminum alloy under various conditions to demonstrate the effects of ultrasonic vibration on the microstructure and mechanical properties of as-cast 7085 aluminum alloy. The distribution of secondary phases and main elements in the as-cast alloy was also investigated. Moreover, the relationship between the microstructure characteristics (e.g. grain size) and mechanical properties (e.g. tensile strength and fracture behavior) was also studied and discussed herein.

2 Experimental

A 7085 aluminum alloy with dimensions ϕ260 mm×800 mm was produced by the semi-continuous casting method. The chemical composition of this alloy (wt%) was detected by inductively coupled plasma-atomic emission spectrometry (ICP-AES), and is presented in Table 1. Several slices (2.3 kg, approximately 0.85 L) of 7085 aluminum alloy were cut from the ingot and introduced into a graphite crucible with a diameter of 134 mm. The alloy was then remelted and held at 780 °C for 1 h in an electrical resistance furnace. After melting, the liquid level in the crucible was approximately 110 mm.

Table 1 Chemical composition of as-cast 7085 aluminum alloy (mass fraction, %)

Zn	Cu	Mg	Zr	Fe
7.29	1.42	1.31	0.11	0.06
Si	Ti	Mn	Cr	Al
0.06	0.009	0.004	0.002	Balance

After cooling the melt to the desired temperature, a preheated radiator was submerged vertically 30 mm deep into the melt. The ultrasonic system included a piezoelectric transducer, a titanium alloy sonotrode of ϕ50 mm×1100 mm, and a cooling fan, as shown in Figure 1. The maximum output power of this ultrasonic system was 2 kW. Thereafter, the metallic melt was subjected to an ultrasonic field for 5 min at a frequency of 20 kHz. During this period, the melt was held at a constant temperature. The temperature at the center on the radiating face was monitored by a thermal couple.

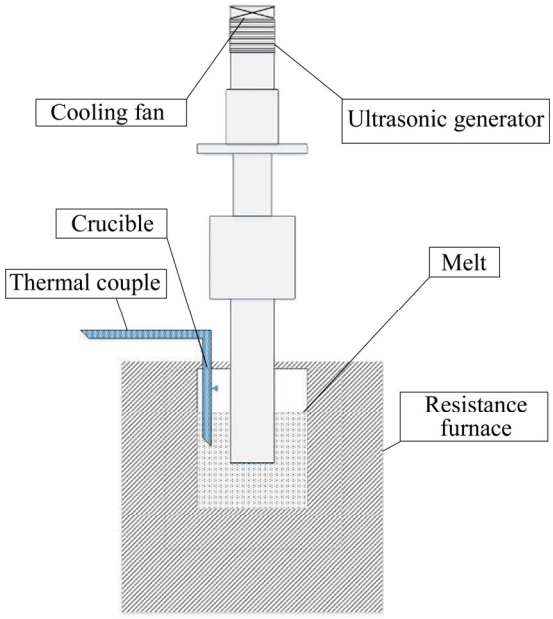

Figure 1 Schematic of ultrasonic casting apparatus

Six groups of experiments were designed specifically as shown in Table 2. Three treatment temperatures were chosen to study the effect of temperature on grain refinement. The minimum heat treatment temperature was 640 °C, because the melt would solidify if the temperature was too low. Moreover, 640 °C is close to the liquidus temperature of this alloy, and the grain size of ingots treated at 640 °C may be quite small, which will be discussed in Section 3.1. Therefore, considering that the grain size may not change significantly with the increase of ultrasonic power at 640 °C, 680 °C (No. 3, 5 and 6 alloys in Table 2) was chosen as the treatment temperature to study the effect of ultrasonic power on grain refinement. Different values of output power were used to generate an ultrasonic field at 680 °C.

After the UST, the molten alloy was poured into a cylindrical iron mold with dimensions of

Table 2 Six groups of alloys treated under different conditions

No.	Temperature/℃	Power/W
1	720	0
2	720	600
3	680	600
4	640	600
5	680	1000
6	680	2000

ϕ60 mm×200 mm. Finally, samples were cut from the center of the ingots. The samples prepared for microstructure characterization were examined by optical microscopy (OM, Leica) and scanning electron microscopy (SEM, FEI Sirion 200). The specimens for OM observation were chemically etched in an anode coating solution (11 g of H_3BO_3, 20 mL of HF, and 1000 mL of H_2O) at 25 V [13]. Grain size was measured by the LAMOS series Imaging Analysis Software using the linear intercept method (Chinese standard GB 6396-2002). The secondary phases were observed in the backscattered electron imaging mode operated at 20 kV. Micro-segregation observations and mapping analyses were performed using EPMA-JAX-8230. The hardness was tested using a Micromets 5104 Vickers hardness tester at 4.9 N for 15 s, and the reported results for each sample represented the average of 10 testing points. Tensile strength was obtained by using the MTS-858 tensile testing machine at a drawing speed of 2 mm/min at room temperature. The fracture surfaces were observed by SEM.

3 Results and discussion

3.1 Microstructure characterization

The microstructures of the selected position, as obtained by optical microscopy, are shown in Figure 2. It can be observed in Figure 2(a), that severe dendrites exist in the conventionally cast sample with an average grain size of 103 μm. The grains in the samples with UST are much finer than in those without UST. The grain size in Figure 2(b) is approximately 83 μm. When UST is performed at 640 °C, the grains are similarly equiaxed crystals with a size of less than 50 μm. Hence, the grain size drops gradually with decreasing treatment temperature.

Acoustic cavitation means that many bubbles

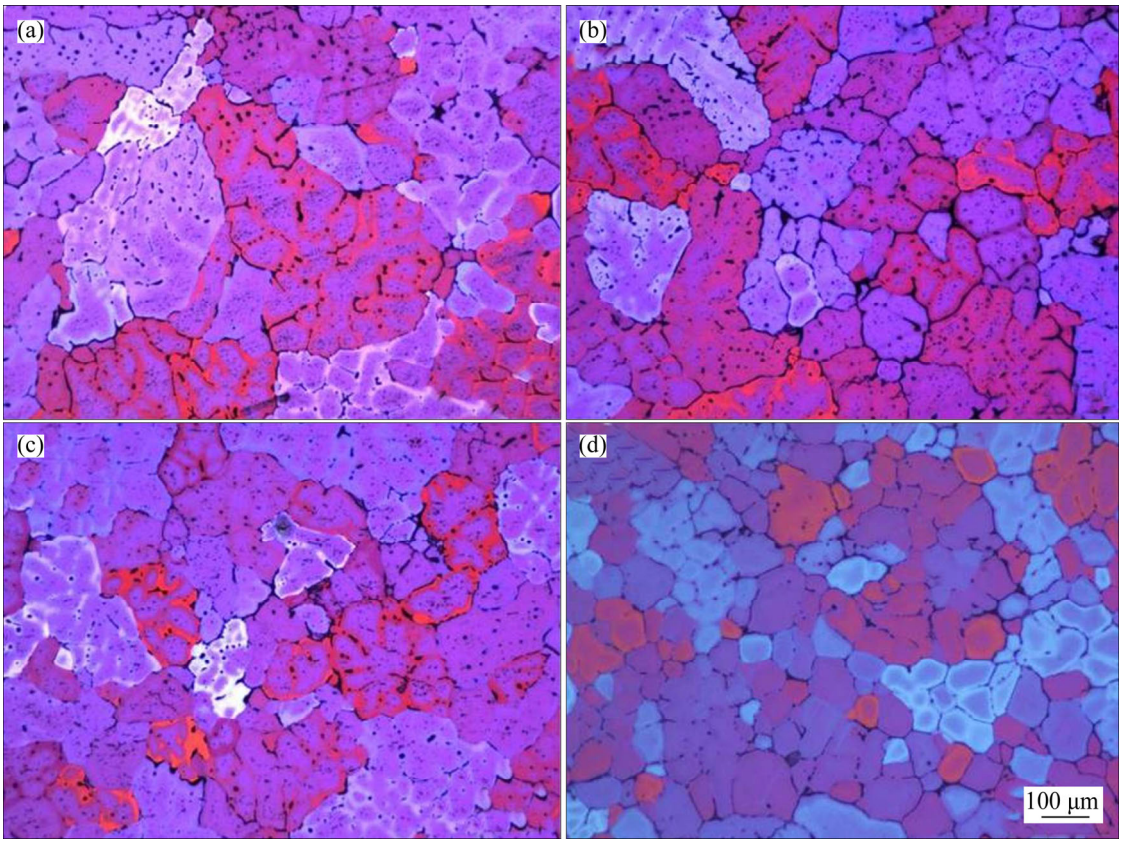

Figure 2 Optical microscopy images of 7085 alloy treated at different temperatures: (a)720 °C, 0 W; (b) 720 °C, 600 W; (c) 680 °C, 600 W; (d) 640 °C, 600 W

are generated under the action of alternating pressure; they initiate in the liquid if the acoustic pressure exceeds the cavitation threshold [14]. Most bubbles collapse after two or three periods of oscillation, which can produce high-temperature spots, high-pressure pulses, and cumulative jets [9, 15]. As a result, a large number of nuclei are produced. On stirring the hot stream, these nuclei get dispersed throughout the melt, and therefore, the primary crystals are much finer because of the enhanced nucleation rate. The effectiveness of UST is influenced by many factors, as reported in literature; for example, the output power used to generate the ultrasonic field [16], amplitude and frequency of ultrasound [17], treatment temperature and duration, and the solidification of conditions [18], i.e. cooling rate, alloy composition, and impurity level. Among all these factors, the treatment temperature range plays an essential role in the efficiency of UST, because the alloy melt viscosity, which is mainly controlled by melt temperature, is one of the major factors that determine the efficiency of UST [19]. The absorption of the liquid phase is determined by the attenuation factor, which is related to the viscosity and thermal conductivity of the melt, and changes with the ultrasound frequency. The attenuation factor [9] is given by

$$\alpha=\frac{\omega^2}{2\rho c^3}\left[\frac{4}{3}\mu+\mu'+\alpha\left(\frac{1}{c_v}-\frac{1}{c_p}\right)\right] \tag{1}$$

where $\omega=2\pi f$ is the angular frequency; ρ is the density of the liquid; c is the propagation velocity of sound; μ and μ' are the shear and volume viscosity, respectively; α is the thermal conductivity. c_v and c_p are the specific heat capacity at constant volume and pressure, respectively. It can be inferred from Eq. (1) that the attenuation factor increases with viscosity. In addition, it is well known that the viscosity of aluminum melt decreases with increasing temperature [20]. Therefore, the efficiency of UST will be lower if the ultrasound is introduced in the melt at higher temperature. The grains of the sample in Figure 2(d) are much finer than those in Figures 2(b) and (c), because the viscosity changes dramatically near the liquidus temperature. Decreasing temperature can lead to a rapid increase in viscosity, which will increase the efficiency of the applied ultrasonic energy.

The microstructure of the samples at the same temperature (680 °C) but at different output powers is shown in Figure 3. The average grain sizes of samples (a), (b), and (c) are approximately 93 μm, 76 μm and 68 μm, respectively. With increasing output power, more cavitation bubbles are generated, and the grain refinement degree increases. Thus, temperature has a greater effect on grain refinement than the output power of ultrasonic sound.

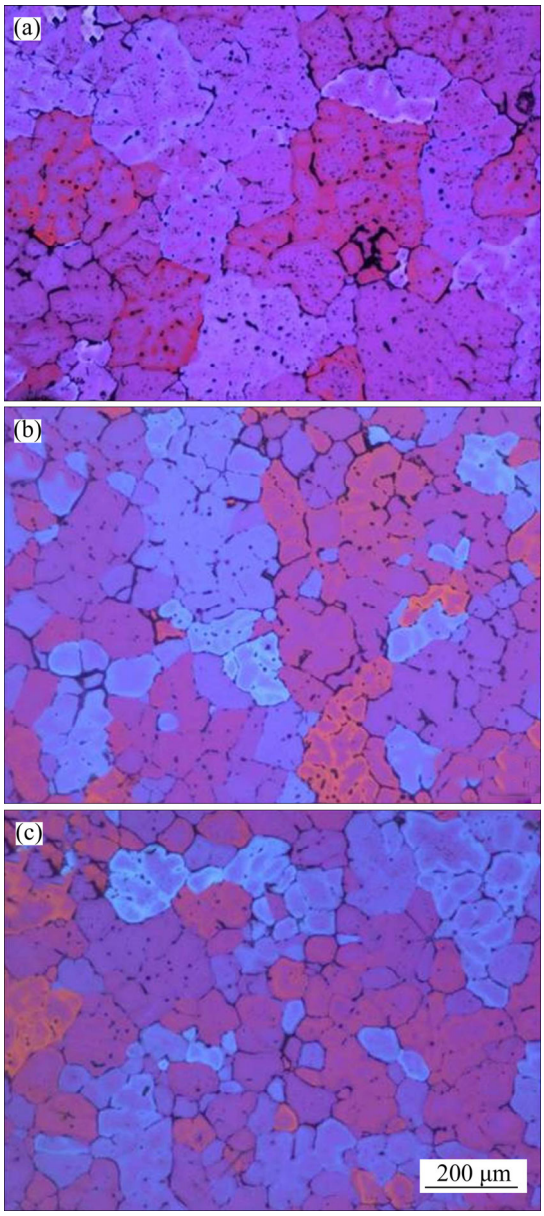

Figure 3 Optical microscopy images of 7085 aluminum alloy treated at different powers: (a) 600 W; (b) 1000 W; (c) 2000 W

3.2 Mechanical properties

To illustrate the effect of UST during solidification on the mechanical properties, the hardness and tensile properties of the different

as-cast samples were assessed and are shown in Figure 4. The Vickers hardness of the cast 7085 alloy without refiner is HV 132, whereas that of the sample treated by ultrasonic sound can reach HV 154. The tensile strength of the sample treated at 780 °C is 225 MPa, which is approximately 50% higher than that of the sample without UST. The improvement of hardness and tensile strength could be a result of the effective grain refinement by introducing ultrasonic sound [21, 22], leading to a finer distribution of secondary phases (i.e., intermetallic) and small grain size. Intermetallic compounds are brittle and are considered important crack-initiating sites during loading [23, 24]; therefore, a finer distribution is beneficial to the mechanical properties. The Hall–Petch relationship is given as [25]

$$\sigma_b = \sigma_0 + k \cdot d^{-\frac{1}{2}} \quad (2)$$

where σ_b is the tensile strength; σ_0 is the lattice friction stress from the dislocation motion; k is the enhancement coefficient; d is the average grain size.

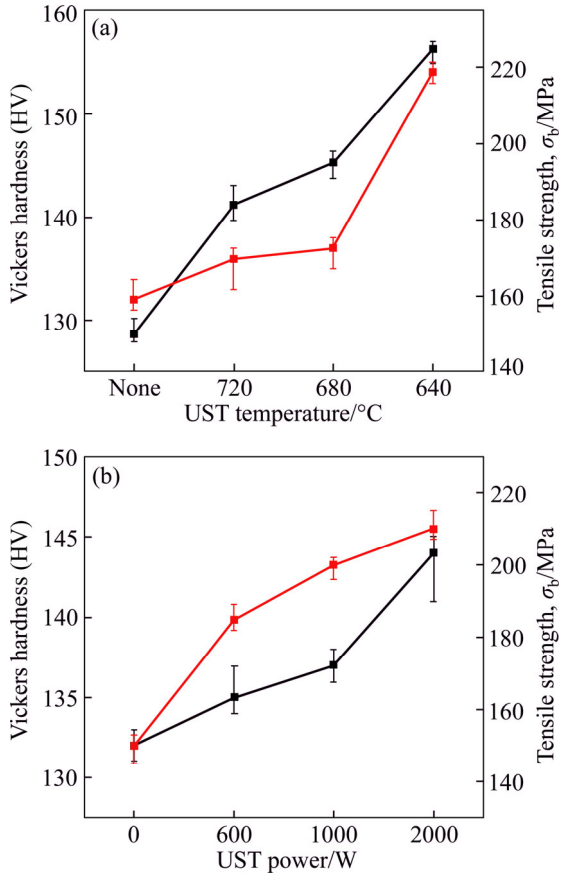

Figure 4 Vickers hardness and tensile strength curves of 7085 alloy: (a) Treated at different temperatures; (b) Treated with different ultrasonic powers

However, σ_0 and k mainly depend on the composition of the alloy. In that case, d, the average grain size, has a determining effect on the tensile strength of the alloy [26]. Therefore, the alloy with UST showed better mechanical performance.

3.3 Morphologies of secondary phases

The SEM morphologies of the 7085 aluminum alloy samples are shown in Figure 5. The intermetallic phases are mainly distributed in the grain boundaries. A mixture of dendrites and lamellar eutectic is observed, and severe segregation exists at the grain boundaries, as shown in Figure 5(a) (without UST). Compared with Figure 5(a), the volume fraction of intermetallic phases in the sample with UST, shown in Figure 5(d), is smaller than that for the conventional as-cast alloy, at 6.03% and 10.71%, respectively. Moreover, there are no dendrites in the sample with UST. It should be also noted in Figure 5(b) that there are secondary phases in the intern of grain in the sample without UST. However, secondary phases are not observed in the corresponding part in the UST sample. The rod-like phases are distributed continuously in the conventionally cast sample, whereas the secondary phases in samples with UST (Figure 5(e)) are discontinuous and look like equiaxed plates.

Under ultrasonic stirring, the volume fraction of the secondary phase decreases significantly, and there is no secondary phase in the center of grains. In the process of solidification, the solutes get mixed by two mechanisms, namely, diffusion and natural convection, and the velocity of the former is much lower than that of the latter. One characteristic of a liquid flowing in a tube is that the velocity near the tube wall is almost zero. Hence, when the aluminum melt is solidifying, there are boundaries without any flow near the tube wall. The same phenomenon also exists in solid–liquid boundaries during solidification; therefore, solutes in boundaries can only diffuse slowly to the convection zone in a melt. Therefore, solutes tend to aggregate at the boundary, as shown in Figure 5. When ultrasound is introduced into a melt, ultrasonic cavitation is initiated, which could produce transient micro "hot spots." These micro "hot spots" can reach very high temperatures, pressures of approximately 101 MPa, and heating and cooling rates above 10^{10} K/s [21]. The strong

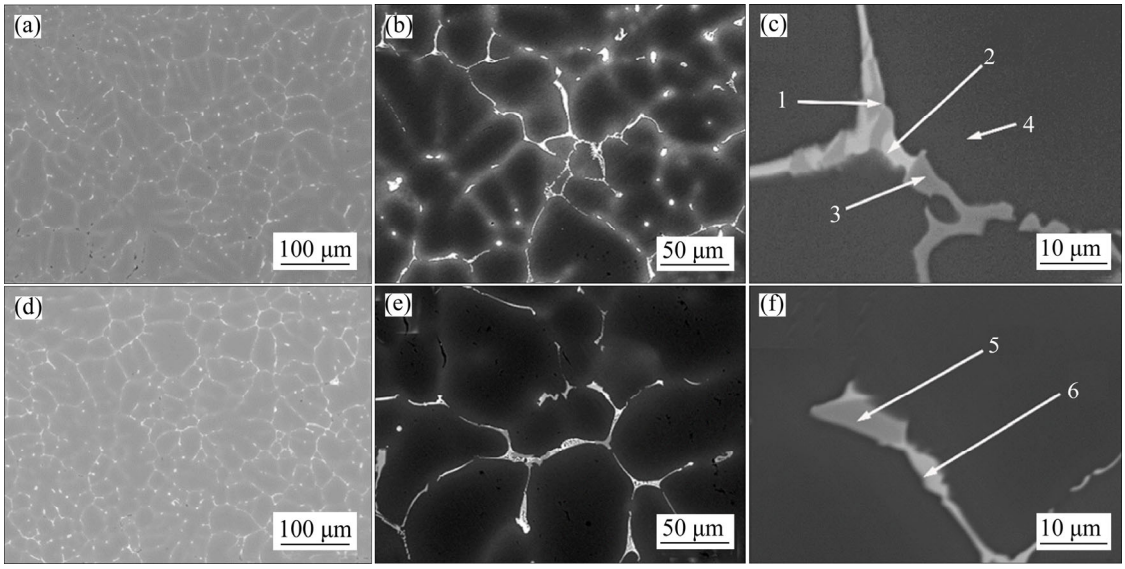

Figure 5 Scanning electron microscopy images depicting morphologies of as-cast alloy: (a, b, c) Without UST; (d, e, f) With UST

impact accompanied by the local high temperature could not only force the exchange of substance between the solid phase and liquid phase, but also break solute clusters [27, 28]. Thus, there are fewer secondary phases in samples treated by ultrasonic sound.

3.4 EDS analysis

EDS was used to analyze the composition of the secondary phases (Figure 5) in the 7085 aluminum alloy, and the results are presented in Table 3. According to the EDS analysis, the lamellar phase in spot 2 of Figure 5 contains 64.43% Al, 27.22% Cu, 3.75% Mg, and 4.33% Zn (molar fraction). Compared to Al and Cu, the concentration of other elements is much lower; therefore, spot 2 is considered to be Al_2Cu. The bright phases (spot 1) close to Al_2Cu are T eutectic. The element concentration in spot 3 is similar to that in spot 5, where the concentration of Fe is higher than that in other places. Hence, it can be concluded that spot 3 and spot 5 are Fe-rich phases. Fe-rich phases can hardly be eliminated because of the high melt temperature of Fe. This implies that ultrasonic sound failed to break the small particles containing a large proportion of Fe. It is obvious that spot 4 is an Al matrix. Similar to spot 1, spot 6 is the T phase. From the EDS analysis, there is little difference between the types of secondary phases in the ultrasonically cast sample and conventionally cast sample, although the volume fraction of secondary phases is obviously reduced.

Table 3 Chemical compositions of secondary phases in Figure 5 (mass fraction, %)

Position	Al	Zn	Mg	Cu	Fe	Others
1	31.58	24.01	26.45	17.75	0.06	0.14
2	64.43	4.33	3.75	27.22	0.10	0.17
3	72.34	2.16	0.21	6.15	15.92	3.17
4	95.18	3.37	1.07	0.32	0.04	0.03
5	71.19	2.36	0.30	11.07	13.70	1.32
6	37.69	20.56	26.84	14.76	0.07	0.83

3.5 Microsegregation

To further investigate the effect of the ultrasonic field on microsegregation, electron microprobe analysis (EPMA) mapping was performed. The use of an electron microprobe micro-analyzer enabled us to obtain the electron microprobe elemental maps for Al, Zn, Mg and Cu (see Figures 6 and 7). The bright color indicates that the concentration of one element is higher in this area. It should be noted that Cu only exists in the grain boundaries in both alloys, because the diffusion coefficient of Cu in Al–Zn–Mg–Cu alloys is smaller than that of Mg and Zn at the same temperature [13, 29]. The concentration of Zn and Mg in grain boundaries in the sample without UST is higher than that in the ultrasonic cast sample. However, there is an opposite trend in areas near the grain boundaries. This implies that zinc and

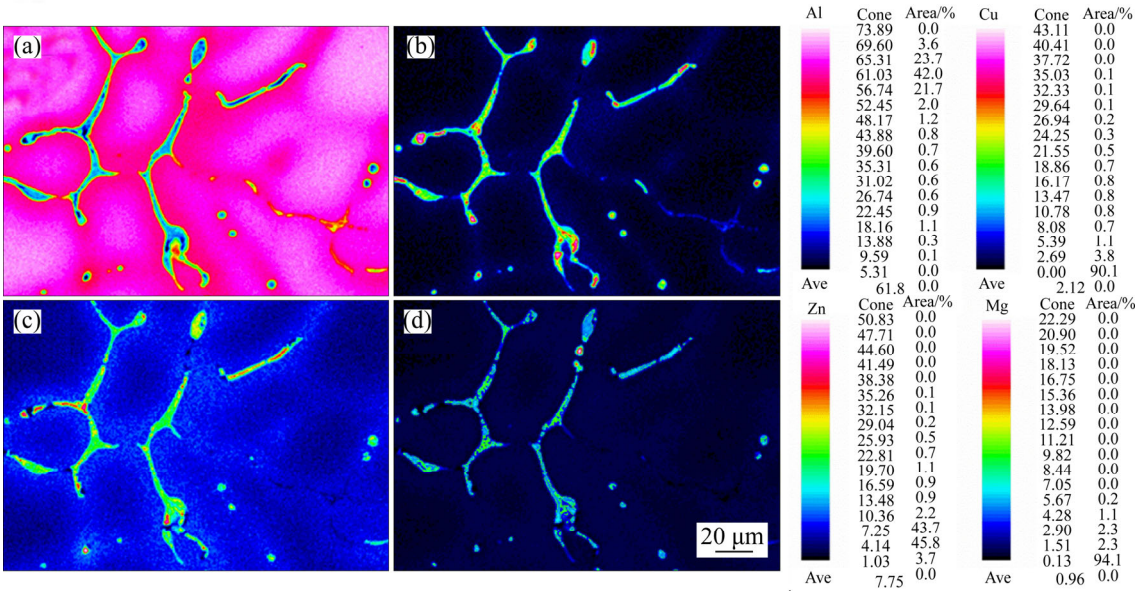

Figure 6 Main elemental distribution in alloy without UST: (a) Al; (b) Zn; (c) Mg; (d) Cu

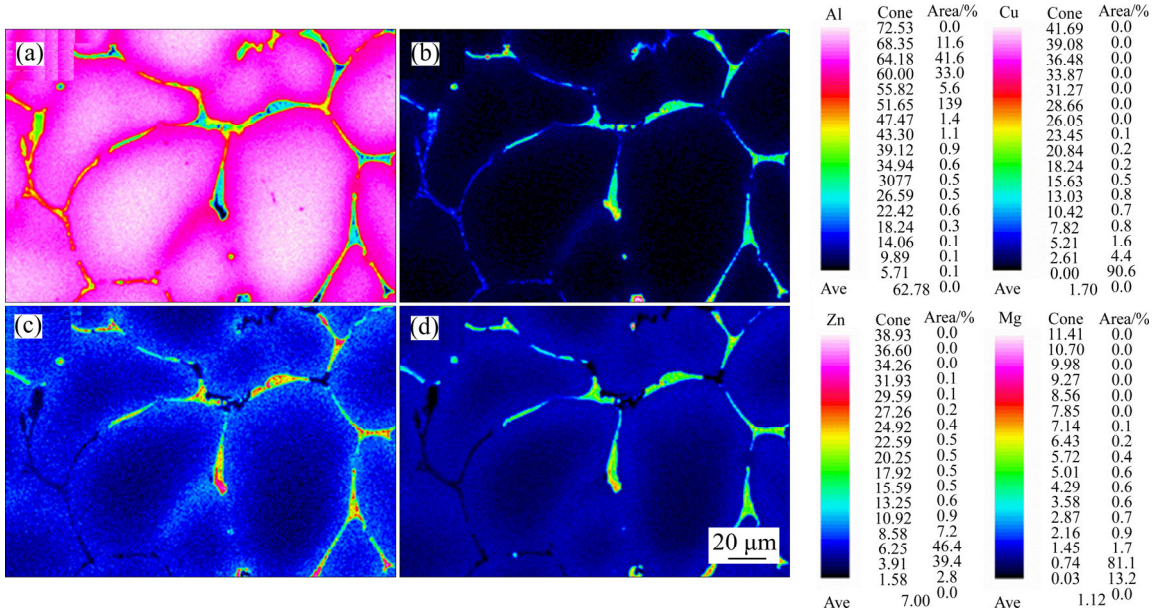

Figure 7 Main elemental distribution in UST-refined alloy: (a) Al; (b) Zn; (c) Mg; (d) Cu

magnesium diffused out of the secondary phase in grain boundaries during UST. This agrees well with the earlier observation that the secondary phases in samples with UST are more discontinuous, as shown in Figure 5.

The results of EPMA mapping indicate that there is severe element segregation in the conventionally cast sample. However, this can be largely reduced by introducing UST. This can be explained by the results in section 3.3, in which micro "hot spots" with high temperature and pressure facilitate substance exchange between a grain boundary and its neighboring area.

3.6 Fracture morphologies

Fracture morphologies are presented to further study the effect of the ultrasonic field on mechanical properties. Figure 8 shows the fracture surface of the as-cast aluminum alloy. Many smooth flat areas can be observed in Figure 8(a), which indicates that fracture of this sample occurred in a brittle manner. The macrofracture of the alloy with UST is shown in Figure 8(d). Compared to Figure 8(a), it can be seen from Figure 8(d) that the fracture surface is more uniform. This pattern represents the appropriate effect (e.g. more homogeneous distribution of second phases, more

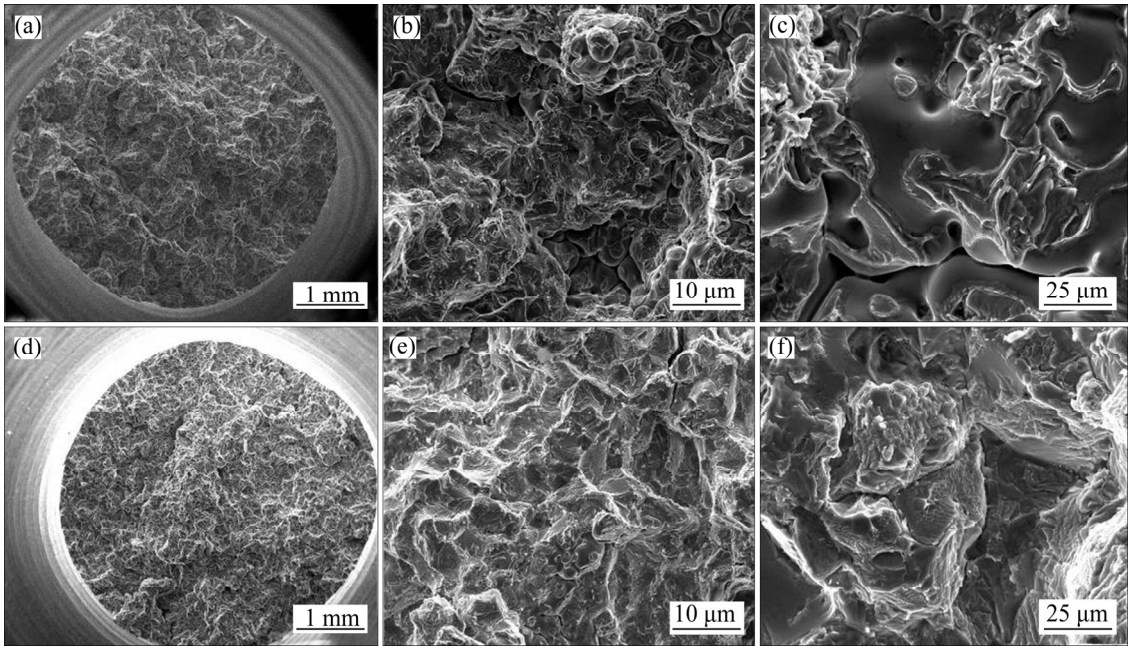

Figure 8 Fracture surfaces of samples at high magnification: (a, b, c) Without UST; (d, e, f) With UST

refined and uniform grains [23]) of UST in 7085 aluminum alloy. As shown in Figure 8(b), the cleavage plane and tearing ridge, which are usually considered to be typical brittle fracture features, can be seen on the surfaces of the as-cast ingots. This is probably because the brittle secondary phases (e.g. intermetallics) that gathered on the grain boundaries destroyed the continuity of the grain boundaries [30, 31]. Moreover, part of the fracture surface has not deformed, as shown in Figure 8(c). However, in Figure 8(e), rupture of the sample with UST occurred in quasi-cleavage fracture. The cleavage plane became smaller and a typical tearing characteristic can be seen, which indicates that the mechanical properties of this alloy greatly improved.

Because of UST during casting, brittle secondary phases tend to be discontinuous. Therefore, there is stronger interaction between slip bands, as compared to that in conventionally cast samples, and plastic flow in the grain boundaries [26]. As a result, the fracture of the eutectic phase (e.g. T phase or θ phase) is more likely to originate in the grain boundaries, and the final fracture path tends to pass through the eutectic phase along the boundaries of the α-Al primary phase. The size of the grains also has a significant effect on the fracture morphologies. The smaller the grain, the more unsmooth the grain surface, which has an adverse influence on crack propagation. Thus, the sample with UST exhibits better mechanical performance. However, ultrasound can degas the molten aluminum. It is well known that the fracture surface of as-cast alloys is usually highly porous due to gas entrapment during die cavity filling [32]. In addition, the mechanical properties of as-cast aluminum alloys depend on several factors, with particular emphasis on the size and distribution of porosities [33]. The fracture path tends to go through the shrinkage porosity because excessive shrinkage porosity defects exist in castings [26]. These areas with porosities will not deform like the matrix when the sample is subjected to tensile tests. Therefore, there are some areas without any deformation in the fractograph of the conventional castings, as shown in Figure 8(c). As stated in section 3.2, the tensile strength of the UST specimen (225 MPa) was 50% higher than that of the specimen produced by conventional casting (150 MPa). The above fracture mechanism is in good accordance with our experimental results in section 3.2.

4 Conclusions

1) After ultrasonic sound is introduced to a 7085 aluminum alloy during solidification, the alloy is significantly refined due to acoustic cavitation. The average grain size decreases from 103 μm to 50 μm. With decreasing treatment temperature, the

average grain size drops sharply. Increasing the output power of the ultrasonic system also leads to grain refinement, and the optimal treatment temperature is 640 °C.

2) The mechanical properties of the 7085 aluminum alloy are improved by application of an ultrasonic field in the melt during solidification. The Vickers hardness and tensile strength increase by 17% and 50%, respectively.

3) The secondary phases in the sample with UST are discontinuous, and their volume fraction decreases significantly. The element distribution in the sample with UST is more homogeneous, and microsegregation of Cu, Zn, and Mg in the grain boundaries is mitigated.

4) From the tensile tests and fracture morphologies, the fracture surfaces of the 7085 aluminum alloy obtained from conventional casting show clear brittle fracture, whereas the fracture of the 7085 aluminum castings obtained with UST occurs in a quasi-cleavage manner.

References

[1] LAI Jian-ping, JIANG Rong-piao, LIU Hua-shan, DUN Xiao-long, LI Yan-fen, LI Xiao-qian. Influence of cerium on microstructures and mechanical properties of Al–Zn–Mg–Cu alloys [J]. Journal of Central South University, 2012, 19(4): 869–874.

[2] LI Xin-wei, CAI Qi-zhou, ZHAO Bing-yi, XIAO Ya-ting, LI Bing. Effect of nano TiN/Ti refiner addition content on the microstructure and properties of as-cast Al-Zn-Mg-Cu alloy [J]. Journal of Alloys and Compounds, 2016, 675: 201–210.

[3] YU Hong-chun, WANG Ming-pu, JIA Yan-lin, XIAO Zhu, CHEN Chang, LEI Qian, LI Zhou, CHEN Wei, ZHANG Hao, WANG Yang-guo, CAI Can-ying. High strength and large ductility in spray-deposited Al–Zn–Mg–Cu alloys [J]. Journal of Alloys and Compounds, 2014, 601: 120–125.

[4] MOHANTY P S, GRUZLESKI J E. Mechanism of grain refinement in aluminium [J]. Acta Metallurgica et Materialia, 1995, 43(5): 2001–2012.

[5] ZHANG Bei-jiang, CUI Jian-zhong, LU Gui-min. Effects of low-frequency electromagnetic field on microstructures and macrosegregation of continuous casting 7075 aluminum alloy [J]. Materials Science and Engineering A, 2003, 355(1, 2): 325–330.

[6] HUNG J C, LIN C C. Investigations on the material property changes of ultrasonic-vibration assisted aluminum alloy upsetting [J]. Materials & Design, 2013, 45: 412–420.

[7] ZHANG Li-hua, YU Jun, ZHANG Xiao-ming. Effect of ultrasonic power and casting speed on solidification structure of 7050 aluminum alloy ingot in ultrasonic field [J]. Journal of Central South University, 2010, 17(3): 431–436.

[8] ZHAO Jun, YU Kun, XUE Xin-ying, MAO Da-heng, LI Jian-ping. Effects of ultrasonic treatment on the tensile properties and microstructure of twin roll casting Mg–3%Al–1%Zn–0.8%Ce–0.3%Mn (wt%) alloy strips [J]. Journal of Alloys & Compounds, 2011, 509(509): 8607–8613.

[9] ESKIN G I, ESKIN D G. Ultrasonic treatment of light alloy melts [M]. Florida: CRC Press, 2014.

[10] YASUDA K, SAIKI Y, KUBO T, KUWABARA M, YANG J. Influence of high-power ultrasonic irradiation on primary nucleation process during solidification [J]. Japanese Journal of Applied Physics B, 2007, 46(7): 4939–4944.

[11] JIANG Ri-peng, LI Xiao-qian, ZHANG Min. Investigation on the mechanism of grain refinement in aluminum alloy solidified under ultrasonic vibration [J]. Metals and Materials International, 2015, 21(1): 104–108.

[12] XU Han-bing, JIAN Xiao-gang, MEEK T T, HAN Qing-you. Degassing of molten aluminum A356 alloy using ultrasonic vibration [J]. Materials Letters, 2004, 58(29): 3669–3673.

[13] SHI Yun-jia, PAN Qing-lin, LI Meng-jia, LIU Zhi-ming, HUANG Zhi-qi. Microstructural evolution during homogenization of DC cast 7085 aluminum alloy [J]. Transactions of Nonferrous Metals Society of China, 2015, 25(11): 3560–3568.

[14] ESKIN G I, ESKIN D G. Production of natural and synthesized aluminum-based composite materials with the aid of ultrasonic (cavitation) treatment of the melt [J]. Ultrasonics Sonochemistry, 2003, 10(4, 5): 297–301.

[15] ESKIN G, PIMENOV Y P, MAKAROV G. Effect of cavitation melt treatment on the structure refinement and property improvement in cast and deformed hypereutectic Al-Si alloys [C]// Materials Science Forum, 1997, 242: 65–70.

[16] TZANAKIS I, LEBON G S B, ESKIN D G, PERICLEOUS K. Investigation of the factors influencing cavitation intensity during the ultrasonic treatment of molten aluminium [J]. Materials & Design, 2016, 90: 979–983.

[17] ATAMANENKO T V, ESKIN D G, ZHANG L, KATGERMAN L. Criteria of grain refinement induced by ultrasonic melt treatment of aluminum alloys containing Zr and Ti [J]. Metallurgical and Materials Transactions A, 2010, 41(8): 2056–2066.

[18] WANG Gui, DARGUSCH M, QIAN M, ESKIN D, STJOHN D H. The role of ultrasonic treatment in refining the as-cast grain structure during the solidification of an Al–2Cu alloy [J]. Journal of Crystal Growth, 2014, 408: 119–124.

[19] WANG Feng, ESKIN D, CONNOLLEY T, MI Jia-wei. Effect of ultrasonic melt treatment on the refinement of primary Al3Ti intermetallic in an Al–0.4Ti alloy [J]. Journal of Crystal Growth, 2016, 435: 24–30.

[20] STRAUSS S. The temperature dependence of the viscosity of liquid metals [J]. Nuclear Sci & Eng, 1962, 18(2): 279–285.

[21] SU Hai, GAO Wen-li, FENG Zhao-hui, LU Zheng. Processing, microstructure and tensile properties of nano-sized Al_2O_3 particle reinforced aluminum matrix composites [J]. Materials & Design, 2012, 36: 590–596.

[22] SHI Chen, MAO Da-heng, FU Zong-li. Effect of electromagnetic and ultrasonic cast rolling on microstructure and properties of 1050 aluminum substrate for presensitized

plate [J]. Journal of Central South University, 2015, 22(2): 422–429.
[23] SEYED EBRAHIMI S H, EMAMY M. Effects of Al–5Ti–1B and Al–5Zr master alloys on the structure, hardness and tensile properties of a highly alloyed aluminum alloy [J]. Materials & Design, 2010, 31(1): 200–209.
[24] KOBAYASHI T. Strength and fracture of aluminum alloys [J]. Materials Science and Engineering A, 2000, 280(1): 8–16.
[25] DIETER G E, BACON D J. Mechanical metallurgy [M]. New York: McGraw-Hill, 1986.
[26] JIANG Wen-ming, FAN Zi-tian, CHEN Xu, WANG Ben-jing, WU He-bao. Combined effects of mechanical vibration and wall thickness on microstructure and mechanical properties of A356 aluminum alloy produced by expendable pattern shell casting [J]. Materials Science and Engineering A, 2014, 619: 228–237.
[27] YAN Jiu-chun, XU Zhi-wu, SHI Lei, MA Xing, YANG Shi-qin. Ultrasonic assisted fabrication of particle reinforced bonds joining aluminum metal matrix composites [J]. Materials & Design, 2011, 32(1): 343–347.
[28] MONTALBA C, ESKIN D G, MIRANDA A, ROJAS D, RAMAM K. Effect of electroceramic particles on damping behaviour of aluminium hybrid composites produced by ultrasonic cavitation and mechanical stirring [J]. Materials & Design, 2015, 84: 110–117.
[29] LI Wen-bing, PAN Qing-lin, XIAO Yan-ping, HE Yun-bing, LIU Xiao-yan. Microstructural evolution of ultra-high strength Al–Zn–Cu–Mg–Zr alloy containing Sc during homogenization [J]. Transactions of Nonferrous Metals Society of China, 2011, 21(10): 2127–2133.
[30] WANG Q G. Microstructural effects on the tensile and fracture behavior of aluminum casting alloys A356/357 [J]. Metallurgical and Materials Transactions A, 2003, 34(12): 2887–2899.
[31] TAHSINI S M, HALVAEE A, KHOSRAVI H. Correlation between microstructural features and tensile strength for friction welded joints of AA-7005 aluminum alloy [J]. Journal of Central South University, 2016, 23(8): 1839–1846.
[32] BAI Y, ZHAO H. Tensile properties and fracture behavior of partial squeeze added slow shot die-cast A356 aluminum alloy [J]. Materials & Design, 2010, 31(9): 4237–4243.
[33] LI Y, LI R. Effect of the casting process variables on microporosity and mechanical properties in an investment cast aluminium alloy [J]. Science and Technology of Advanced Materials, 2001, 2(1): 277–280.

(Edited by FANG Jing-hua)

中文导读

超声场对 7085 铝合金微观组织和力学性能的影响

摘要：本文采用金相显微分析(OM)、维氏硬度测试、扫描电子显微分析(SEM)、拉伸性能测试和电子探针分析（EMAP）等方法研究熔铸过程中导入超声场对 7085 铝合金铸锭的微观组织、力学性能的影响。结果表明，在超声处理（UST）的作用下，铝合金的晶粒显著细化，同时第二相也更加分散。从 EPMA 的结果中观察到，经过超声处理合金中的 Al、Zn、Mg 和 Cu 元素分布更加均匀。铝合金的力学性能也极大增强。从拉伸断口图中得出，常规铸锭试样的断裂方式是脆性断裂，而超声铸锭试样是以准解理的方式断裂的。

关键词：超声处理；晶粒细化；微观组织；第二相